geosciences

MDPI

Article

Pressure Controlled Permeability in a Conduit Filled with Fractured Hydrothermal Breccia Reconstructed from Ballistics from Whakaari (White Island), New Zealand

Ben M. Kennedy [1,*], Aaron Farquhar [2], Robin Hilderman [2], Marlène C. Villeneuve [1,3], Michael J. Heap [4], Stan Mordensky [1], Geoffrey Kilgour [5], Art. Jolly [5], Bruce Christenson [5] and Thierry Reuschlé [4]

1 Department of Geological Sciences University of Canterbury, Private Bag 4800, Christchurch 8140, New Zealand; marlene.villeneuve@unileoben.ac.at (M.C.V.); stan.mordensky@gmail.com (S.M.)
2 Colorado College, Colorado Springs, Colorado, CO 80903, USA; farquharaaron@gmail.com (A.F.); robinhilderman@gmail.com (R.H.)
3 Chair of Subsurface Engineering, Montanuniversität Leoben, Erzherzog Johann-Straße 3, A-8700 Leoben, Austria
4 Université de Strasbourg, CNRS, Institut de Physique de Globe de Strasbourg UMR 7516, F-67000 Strasbourg, France; heap@unistra.fr (M.J.H.); thierry.reuschle@unistra.fr (T.R.)
5 GNS Science, 1 Fairway Drive, Lower Hutt 5011, New Zealand; G.Kilgour@gns.cri.nz (G.K.); a.jolly@gns.cri.nz (A.J.); B.Christenson@gns.cri.nz (B.C.)
* Correspondence: Ben.kennedy@canterbury.ac.nz

Received: 24 March 2020; Accepted: 8 April 2020; Published: 11 April 2020

Abstract: Breccia-filled eruption conduits are dynamic systems where pressures frequently exceed critical thresholds, generating earthquakes and transmitting fluids. To assess the dynamics of breccia-filled conduits, we examine lava, ash tuff, and hydrothermal breccia ballistics with varying alteration, veining, fractures, and brecciation ejected during the 27 April 2016 phreatic eruption of Whakaari/White Island. We measure connected porosity, strength, and permeability with and without tensile fractures at a range of confining pressures. Many samples are progressively altered with anhydrite, alunite, and silica polymorphs. The measurements show a large range of connected porosity, permeability, and strength. In contrast, the cracked samples show a consistently high permeability. The cracked altered samples have a permeability more sensitive to confining pressure than the unaltered samples. The permeability of our altered ballistics is lower than surface rocks of equivalent porosity, illustrating that mineral precipitation locally blocked pores and cracks. We surmise that alteration within the conduit breccia allows cracks to form, open and close, in response to pore pressure and confining pressure, providing a mechanism for frequent and variable fluid advection pulses to the surface. This produces temporally and spatially variable geophysical and geochemical observations and has implications for volcano monitoring for any volcano system with significant hydrothermal activity.

Keywords: alteration; porosity; eruption; fracture; permeability

1. Introduction

The tragic events on November 2019 at Whakaari (White Island; New Zealand), which killed over 20 people, highlight the need for a better understanding of the controls on phreatic eruptions. In particular, the behaviour of breccia-filled conduits remains a potentially controlling factor on the pressurization timescales and total pressure build-up. Many large volcanic eruptions begin with a

phreatic/hydrothermal eruption that is responsible for clearing a pathway for magma to reach the surface [1]. Similarly, shallow intrusions and economically significant mineral resources are frequently associated with hydrothermal breccia sheets and pipes [2]. The physical properties of these breccia filled conduits is thus critical to volcano monitoring and economic mineral exploration.

The physical properties of the altered materials that fill hydrothermal conduits directly control (1) magma outgassing efficiency, (2) the build-up of pressure that can lead to explosive eruptions [3], and (3) subsequent fluid flow, hydrothermal alteration, and mineralization. Past studies of magmatic conduits and breccias reveal insights into magma flow, outgassing, and fragmentation processes [4–7]. Detailed studies of hydrothermal breccia filled conduits, however, are dispersed between the maar diatreme, hydrothermal mineralization, and petroleum basin literature [2,8–11] and are rarely applied to eruption models.

Until now, studies have described the physical properties of rocks collected from the crater floor of Whakaari to understand their mechanical behaviour and permeability [12,13] and to interpret fragmentation [14], however, these rocks may not be representative of the material filling the vent. Instead, the physical properties of volcanic ballistic samples can be used to provide insight into conduit processes [15]. Therefore, the ballistic field of the 2016 eruption [16] provides a unique opportunity to directly sample the pre-eruption conduit and the magmatic hydrothermal interface beneath the crater at Whakaari. Here, we combine the exceptional altered ballistic samples with established rock mechanical methods to make implications that can be directly applied to an active hazardous volcano.

Whakaari is an andesite stratocone, whose peak emerges 300 m from the Pacific Ocean 48 km off the east coast of New Zealand. The magmatism is the product of oblique western subduction of the Pacific plate under the Australian plate. Whakaari has been New Zealand's most active volcano in recent history. The most recent magmatic and hydrothermal eruption period has lasted from 1976 until present exhibiting a range of magmatic, phreatomagmatic, and hydrothermal eruptions [16,17]. Whakaari has undergone a complex sequence of unrest and minor eruptions since 2011. Geophysical [18–20], geochemical [21], and observational studies [22] reveal a complex interplay between a shallow magmatic system and surface hydrology with volcanic activity modulated by a variably permeable hydrothermal system. Magmatic gas is transferred [23] towards the surface via branching pathways to a series of vents and fumaroles [21]. This model is consistent with studies of hydrothermal vents elsewhere in New Zealand [24]. Quantifying the material properties and the gas transfer mechanisms is critical to developing realistic geophysical and fluid chemistry models and to understanding the hydrothermal magmatic interface with particular relevance to andesite volcanoes with well-developed hydrothermal systems.

Investigating the nature of the rocks that surround magma bodies allows for the interpretation of geophysical signals. For example, volcanic eruptions have been successfully forecast using volcanic earthquakes [25–29]. Earthquake types are inherently tied to the physical properties of the material they travel through [23,30] and the fluid within any cracks [31]. Similarly, models of deformation [20,32] and fluid flow [33] are reliant on the physical properties of conduits and volcanic edifice. During the current period of unrest at Whakaari, geophysical, geochemical, and geological phenomena seen at the surface are interpreted as a direct result of fluids travelling through variably altered volcanic rock.

Alteration affects the physical properties of volcanic rocks [34–37]. Alteration may drive the loss of porosity and permeability via mineral precipitation in pores and cracks [3,37,38] and/or cementation [39]. Reductions in porosity due to alteration can promote brittle behaviour [39]. Conversely, alteration may drive dissolution and pore creation with measurable porosity and permeability increase [40,41] and promote a ductile failure mode [38,42,43]. Additionally, microcracking is a critical textural consequence of alteration related processes. Fractures in volcanic environments typically form in response to tectonic, intrusive, hydration, or thermal forces [44–46], however, they can also form in response to specific thermally-driven mineral reactions and drive porosity/permeability changes [47,48]. Cracks are an important textural consideration in volcanic conduits, and their influence on, for example, the physical

properties of rocks may be highly dependent on lithology and confining pressure, particularly in altered volcanic rocks [37,46,49–52].

Here, we present textural and petrological characteristics of volcanic ballistic samples from the 27 April 2016 hydrothermal eruption of Whakaari. We then present strength, porosity, and permeability variations as a function of confining pressure (i.e., depth). These data are compiled into a conceptual model in which transient cracks control fluid flow in an altered breccia-filled conduit.

2. Materials and Methods

2.1. Sampling and Sample Preparation

Ballistics were collected from various sites 15–200 metres from the rim of Whakaari's crater lake (Figure 1a) during several brief visits following the 27 April 2016 eruption by Kilgour, Farquhar, and Christenson on 2 May, 2 June, and 9 June, 2016 [53]. Three short sampling missions from three different scientists minimised individual exposure following protocol outlined in [54]. A quantitative analysis of a statistically relevant sample set of ballistic lithologies in the field via photo survey was not possible due to the partially buried and discoloured nature of the ballistics and the limited time for systematic sampling within the Health and Safety Risk considerations of GNS Science and University of Canterbury (Figures 1c and 2) [16]. Further, our sampling was biased towards ballistics that were suitable for cutting and drilling (>10 cm max. diameter) (Figure 2). We also include some additional (nonballistic) measurements made on samples of lava, ash tuff, and sulfur cemented tuff collected from surfaces exposed in 2015 (location details provided in [12,13].

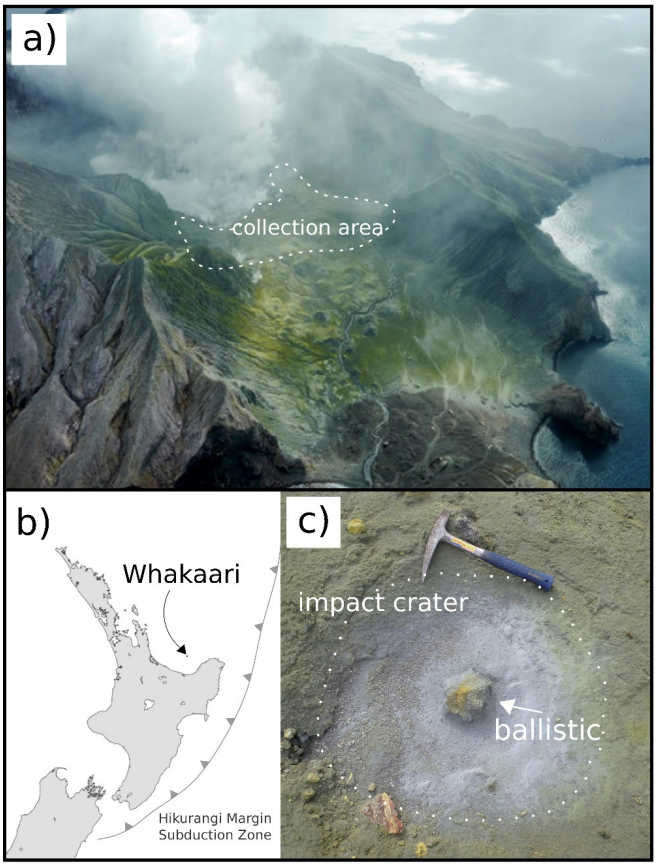

Figure 1. (**a**) Whakaari's crater lake with ballistic collection area highlighted; (**b**) location of Whakaari north-east of the central North Island of New Zealand; (**c**) typical ballistic crater showing discoloration and partial burial of the ballistic.

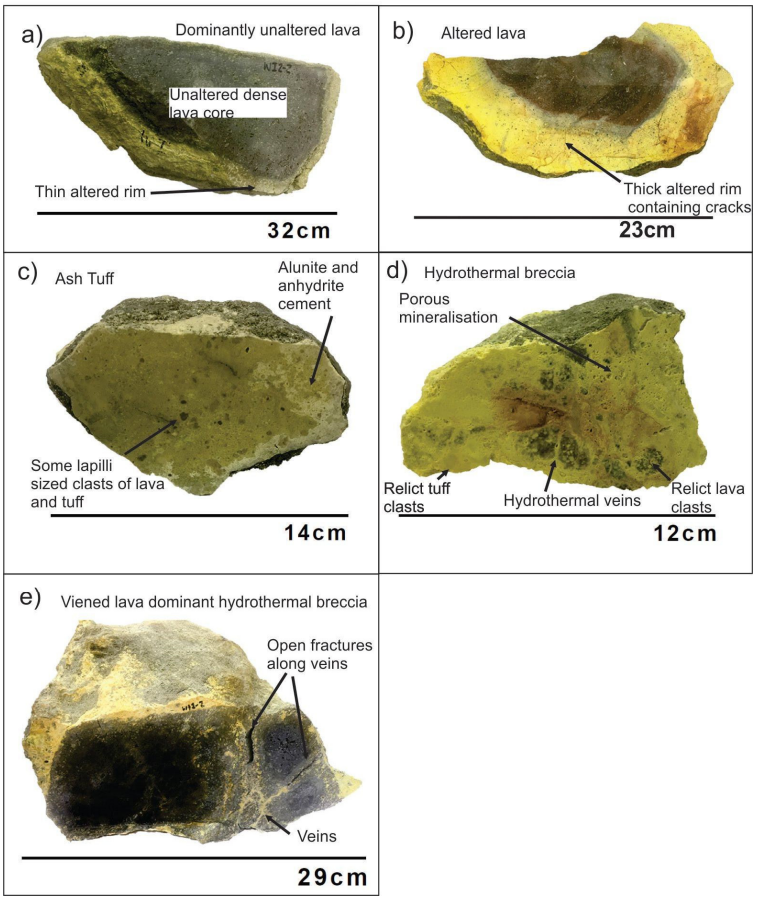

Figure 2. Photographs showing examples of collected ballistic samples from the 2016 eruption at Whakaari cut in two to reveal interior, (**a**) Unaltered lava, (**b**) altered lava, (**c**) Ash Tuff, (**d**) Hydrothermal breccia, (**e**) hydrothermal breccia of altered and unaltered lava.

The collected blocks were subsampled by drilling 20 mm diameter cylinders nominally 20–40 mm long. After porosity and permeability were measured on these intact samples, electrical tape was wrapped around the cores and they were loaded diametrically in compression until the appearance of a through-going tensile macrofracture (i.e., a "Brazilian" indirect tensile test). The tape ensured that the two sample halves remained in contact upon failure, so that the permeability of the fractured samples could be measured in the laboratory (following the method described in [49]).

An ideal methodology would have allowed all samples to have been analysed using all methods. However, this was not possible, due to (1) the timing of availability of samples and experimental facilities across four institutions, three countries, and three student projects, (2) the destructive nature of some of the methodologies (e.g., XRD and accidental sample destruction during drilling), (3) available time for analysis. Our focus was on characterising the permeability and porosity of the rocks that comprised the conduit and encompassing the major breccia lithologies. We made 60 permeability measurements at 3 MPa confining pressure following the standard procedure at University of Canterbury, and a further 25 measurements were done at 1 MPa (following the standard procedure at the University of Strasbourg); all of these had a corresponding connected porosity measurement (Table S1 supplemental data). Nine samples were selected for the two series of time-consuming variable confining pressure experiments: one series without fractures and then the same samples used in the second series with tensile fractures (Table S2 Supplemental data). A subset of 17 of these were chosen for uniaxial compressive strength (UCS) tests (Table S3 Supplemental data). Individual sample numbers and lithological groupings are reported in the supplemental data.

Fifteen thin sections were selected for SEM analysis, and 18 samples were chosen for XRD analysis. These samples were selected to represent the range of lithologies and styles of alteration and allow some overlap of techniques on the same sample. We focus our presentation here on representative samples and textures.

2.2. SEM and XRD Preparation and Methods

Thin sections were prepared to dimensions of 25 × 47 mm, ground to 30 µm thick, and mounted without cover slips. Most samples contained variability in alteration degree, and whenever possible, thin sections were prepared so as to include both sides of these mineralogical boundaries. Thin sections of eight samples were analyzed using a JEOL-IT300 Scanning Electron Microscope (SEM). This was to determine the mineral composition of the rock and the infill in open pore spaces. Backscatter Electron Detector Contrast (BED-C) images and Energy Dispersive X-ray Spectroscopy (EDS) analyses were obtained with images collected at various scales ranging from 60× to 600× magnification, although our results here display all 100× images. The weight-percent ratios of elements within points of each thin section were measured using the EDS detector in order to calculate mineralogy. Compositional element maps (EDS) and lithological structures (BED-C) were produced using the computer program AZtec.

The mineralogy of rock powders and also clay separates were analysed using a Philips PANalytical X'Pert Pro X-ray diffraction (XRD) machine, using X-rays at 2θ angles of 7–70°. Dislodged electrons were received through a 1⁄4° slit. Data were received into the PANalytical computer software Data Collector and then processed to determine mineralogy in the PANalytical computer software High Score.

Two factors were combined in order to determine the most likely mineralogy of each sample. (1) The d-spacing peaks of the minerals within the sample were cross-referenced within the mineral database in High Score to generate a list of possible minerals. (2) Their likelihood of presence within the volcanic-hydrothermal system in combination with existing SEM data. The most abundant peaks for each sample (>50%) were considered a dominant mineral.

In order to determine which clays are present in the ballistic samples, the clays were physically separated from powders onto glass slides. Ten grams of each sample were measured on a precision scale and mixed with 200 mL of distilled water. This was mixed in a Waring blender for two minutes at high power. After mixing, the liquid and fine fraction of the mixture was rapidly decanted into a beaker. This sample was then placed into a 50 mL centrifuge tube and centrifuged at 750 rpm for two minutes. The centrifuged sample was quickly decanted into a second 50 mL tube, which was also centrifuged. This liquid was decanted, and the clay fraction at the bottom of the tube was suctioned out by pipette and placed onto a glass slide. This was placed in the oven at 90 °C for at least one hour, until the sample was dry and ready for XRD analysis. When running clay separation slides, 2θ angles of 5–65° and a 1⁄8° slit were used.

2.3. Physical Laboratory Measurements

Skeletal volume measurements were undertaken using an AccuPyc II 1340 pycnometer. We used helium and ultra-high purity nitrogen for the measurements performed at the Institut de Physique du Globe at the University of Strasbourg (IPGS; France) and the University of Canterbury (New Zealand), respectively. These values were used to calculate connected porosity using the bulk sample volume.

Samples (20 × 20 mm) of unaltered intact lava (WI20 series) and fractured lava (WI20 series) and high-permeability ballistic samples (20 mm in diameter and nominally 20–40 mm in length) were measured at the IPGS. Permeability was measured using a benchtop gas (nitrogen) permeameter (see Farquharson et al., 2016; Heap and Kennedy, 2016). The oven-dry samples were first allowed to equilibrate for one hour at the target confining pressure of 1 MPa (the confining fluid used was also nitrogen gas). We used the pulse-decay technique to measure the intact lava samples and the steady-state method to measure the fractured lava and porous ballistic samples. For the pulse-decay measurements, a pore pressure differential of 0.2 MPa (measured using a Keller pressure transducer) was first imposed on the sample for a duration of one hour. The valve to the gas bottle was then

closed and the decay of the upstream pore pressure (within a known volume) across the sample was recorded as a function of time. These data were then used to assess permeability using Darcy's law and to check for any ancillary corrections, such as the Forchheimer and Klinkenberg corrections, which were applied on a case-by-case basis [55]). These pulse-decay measurements required the Klinkenberg correction. For the steady-state measurements, steady-state volumetric flow rates were measured using a Bronkhorst gas flowmeter for six different pressure differentials. Steady-state was ensured by waiting for the volumetric flow rate and differential pressure to stabilize before measurements were recorded. These data were then used to assess permeability using Darcy's law and to check for any ancillary corrections, such as the Forchheimer and Klinkenberg corrections, which were applied on a case-by-case basis. These steady-state measurements required the Forchheimer correction.

Samples (20 × 20 mm) of unaltered intact lava (WI20 series) and fractured lava (WI20 series) were also measured at IPGS up to a confining pressure of 30 MPa. These experiments used either the pulse-decay (for low-permeability measurements) or the steady-state method (for high-permeability measurements), using the techniques described above. For these measurements, water was used as the confining fluid and argon gas was used as the pore fluid. The confining pressure was only increased to the next increment after the permeability of the sample was measured to be the same on two consecutive days.

Low-permeability 20 mm diameter by nominally 20–40 mm length cores of lava, altered lava, altered ash tuff, hydrothermal breccia, and fumarolic sulfur flow (Table 1) were measured in a Core Laboratories Pulse Decay Permeameter-200 and analyzed using the software PDP V2.75 at the University of Canterbury Rock Mechanics Laboratory. Each oven-dried core was slid into a permeameter sleeve, and a hand pump was used to move Penrite ISO46 hydraulic oil into a surrounding chamber which set the confining pressure to 3 MPa. This pressure corresponds to the confining pressure that the rock experienced within the shallow subsurface [13]. The system was then left to equilibrate for at least thirty minutes. The calculations of connected porosity, mass, dimensions of the core, and atmospheric conditions such as temperature and barometric pressure values acted as a necessary input into the PDP software before running each set of tests. After entering these data, the computer automatically pressurized the chamber from above with high purity nitrogen gas, creating a pressure differential of 10 PSI between the top of the sample and the bottom. The rate at which the sample equilibrated to matching pressures above and below the sample was used by the permeameter calculator to determine the permeability of the sample, as described by [40].

Table 1. X-ray diffraction data for the samples studied.

Sample Type and Numbers	XRD Peaks Identified
Unaltered Lava (n = 3), unaltered portions from samples 1-2, 2-2, 2-4	Labradorite, Anorthoclase, Anhydrite, Alunite, Pyrite, Cristobalite, Zaherite *
Altered Lava (n = 4) altered portions from samples 2-1, 2-4, 3-2, 161-8,	Albite, Opal Anhydrite Alunite Cristobalite, Zaherite *, Gyrolite *
Altered Ash Tuff (n = 5) 3-3, 1-1, 3-1, 3-4, 3-7	Cristobalite Alunite, Tridymite Rectorite *, Montmorillonite *,
Hydrothermal Breccia (n = 5) 2615-4, 2-3, 163-2b, 161-22, 3-5 Surge matrix	Alunite, Anhydrite, Cristobalite, Pyrite, Zaherite *, Gyrolite * Cristobalite, Labrodorite

* Clay found using clay-separation method, not performed on all XRD samples.

The permeability of the fractured low porosity rock cores was measured in the steady-state gas permeameter at the University of Canterbury. The cores dwelled at 1 MPa confining pressure for 30 min in a Hoek cell and a compression frame as high purity nitrogen gas flowed through the sample at 4 bar to equilibrate the pressure. The volumetric gas flow rate was increased five times without exceeding 500 mL/min to reduce the risk of potential damage to the flow meter from broken fragments

of the core entering the downstream tube and to reduce the deformation of the fractures themselves. The Forchheimer correction was applied to correct for flow inertia (as described in [55]).

Nine samples were tested under varied confining pressure, which was increased to mimic the environment of increasing depth of the conduit of Whakaari. These variable pressures simulate different hydrostatic pressures at Whakaari from about 300 m to 3 km depth and follow the same methodology as above and described in [40]. The Forchheimer correction was applied at each of these confining pressure steps.

2.4. Mechanical Laboratory Measurements

Select oven dried core samples from a wide range of lithologies and degrees of alteration (Table 1) were placed in a Tecnotest KE300/ECE compression loading frame to measure their uniaxial compressive strength (UCS), where $\sigma_1 > 0$ and $\sigma_2 = \sigma_3 = 0.1$ MPa (atmospheric). To measure UCS, a 20 mm diameter x 40 mm long core sample was placed between the machine's two platens, which then deformed the sample at a constant displacement rate of 0.03 mm/s. Macroscope failure of the sample was signalled by the formation of a through-going fracture, corresponding to a rapid decrease in stress. The peak axial stress achieved during the experiment was taken as the UCS.

3. Results

3.1. Lithologies

We focus our analysis on relatively unaltered lava from the surface, ballistics (unaltered lava, altered lava, altered tuff, and hydrothermal breccias), and sulfur cemented tuff from surface fumaroles [13]. The relatively unaltered lava blocks had some combination of very thin alteration rinds (Figures 2a and 3a) and central portions that were unaltered allowing unaltered cores to be subsampled (Figure 2b). Textural and compositional analyses reveal low porosity with unaltered phenocrysts of pyroxene, plagioclase, and iron oxides, and microlites of plagioclase and pyroxene, typical of Whakaari lava [56]. Porosity is observed to be mainly created by open macro- and microcracks (Figure 3a).

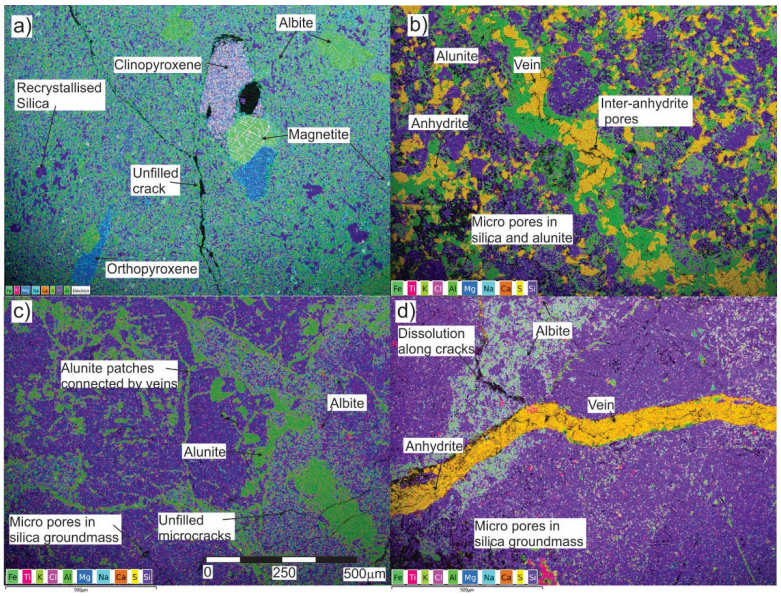

Figure 3. Scanning Electron Microscopy EDS (Energy Dispersive X-ray Spectroscopy) element maps of (**a**) relatively unaltered lava; (**b**) altered lava; (**c**) altered lava; (**d**) altered lava. Note that the scale of each image is the same as in (**c**).

Altered lava cores were drilled from yellow or white ballistics, from partial or complete alteration rinds thicker than 2 cm (Figure 2b). Alteration of the albite microlite rich lava groundmass has resulted

in a crystallised microporous groundmass of silica polymorphs. Macrofractures and macropores are enlarged by dissolution and completely replaced, forming anhydrite and alunite veins, pockets (Figure 3b,d), or more diffuse areas partially replaced with alunite (Figure 3c). Larger pores contain coarser recrystallized grains of anhydrite (Figure 3b).

Ballistics of pyroclastic rocks were also found: altered ash tuff, lapilli tuff and tuff breccia (Figure 2c,d). These ballistics were completely altered to a yellow or white colour rather than just on their surfaces. Such pervasive alteration makes clasts and matrix hard to distinguish in hand specimen, due to their similar texture and mineralogy. The matrix/cement consists of <1 mm recrystallized silica polymorphs (Figure 4a), large areas of alunite (Figure 4a), and local areas of anhydrite (Figure 4b) and some clay minerals identified in XRD. Clasts are tuff, or occasional recrystallized coarser grained lava with albitic patches (Figure 4b). Clasts and matrix are relatively porous with pores existing between recrystallized grains (Figure 4c,d).

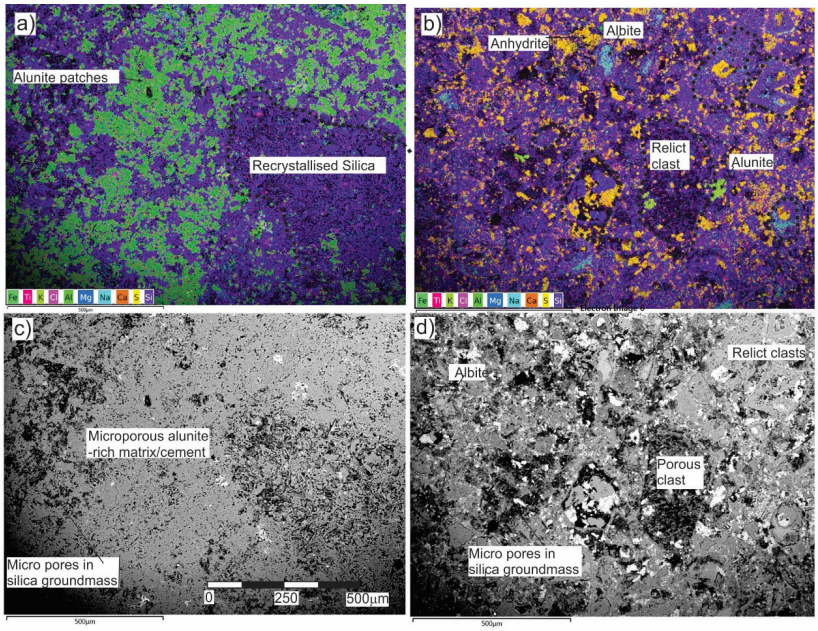

Figure 4. Scanning Electron Microscopy EDS (Energy Dispersive X-ray Spectroscopy) element maps and backscatter images, respectively, of (**a**) and (**c**) ash tuff matrix of a hydrothermal breccia from block 2-3; (**b**) and (**d**) ash tuff block 3-3.

Many ballistics consist of large clasts with only patches of matrix and were significantly mineralised and as such are described here as hydrothermal breccias. A large proportion of these samples are recrystallized and are frequently made up of more than 50% hydrothermal minerals such as alunite or anhydrite (Figure 2d,e and Figure 5b,c). Elemental sulfur is rare but does occur in small patches (Figure 5b). Texturally characteristic cristobalite with fishscale style fractures also occurs, while porous cristobalite is also seen in some vein margins (Figure 5c,d). Multiple generations of alunite and anhydrite veins are seen producing in-situ brecciation of clasts. Fractures are also observed within veins, or parallel to pre-existing fractures, and at the boundary between veins and stronger silicic clasts (Figure 5f). It is also worth noting the contrasting porosity in the vuggy anhydrite, the microporous lava, and the characteristic fishscale cracked cristobalite.

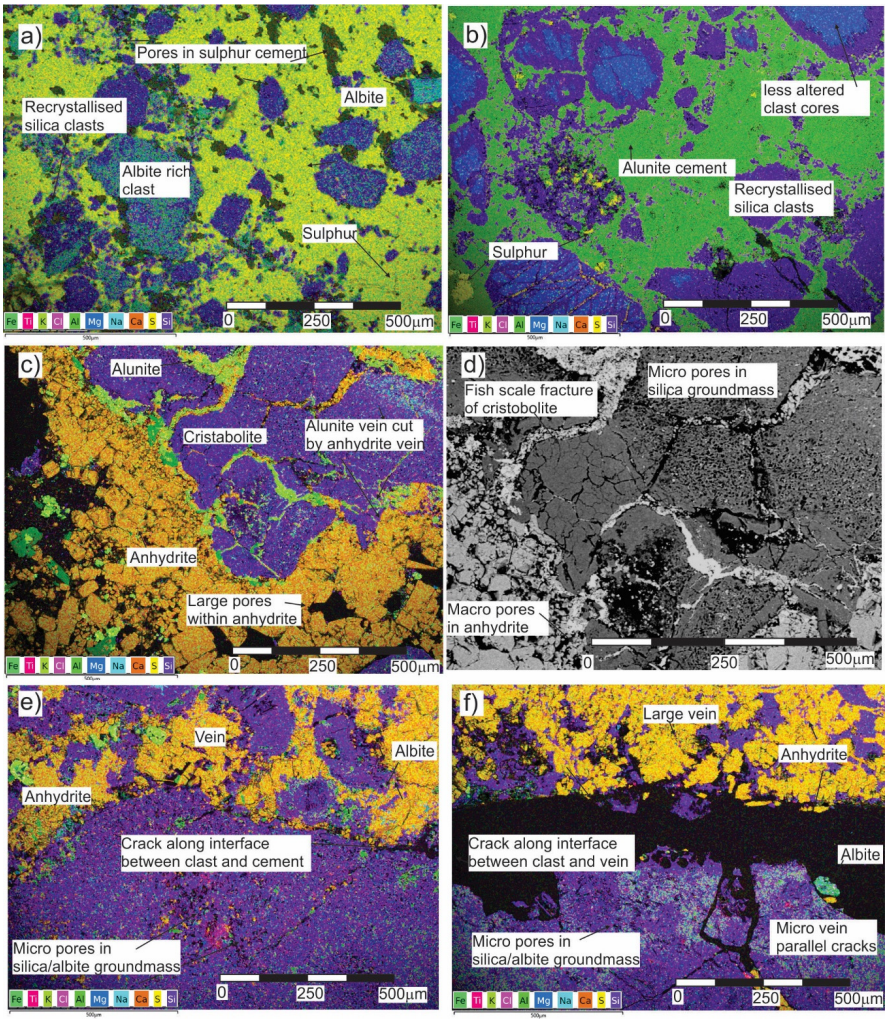

Figure 5. Scanning Electron Microscopy EDS (Energy Dispersive X-ray Spectroscopy) element maps of (**a**) EDS stacked image of sulfur cemented ash tuff; (**b**); EDS stacked image of alunite cemented portion of hydrothermal breccia (**c**) EDS element map of hydrothermal breccia; (**d**) same sample as (**c**) in backscatter to highlight porosity distribution (**e**) EDS stacked image of hydrothermal breccia (**f**) EDS stacked image of open vein in hydrothermal breccia.

These samples are additionally compared against data and textural observations of sulfur encrusted and cemented ash tuff from the surface. These yellow rocks are dominantly matrix supported and cemented with sulfur and contain angular ash and lapilli sized clasts of silica polymorphs and albite and irregular rounded pores resembling vesicles (Figure 5a).

3.2. Porosity and Permeability

Porosity for the entire sample set varies from a couple of percent up to ~60%, and permeability varies from ~4×10^{-19} to ~4×10^{-15} m^2 (Figure 6). Although there is a general trend of increasing permeability with increasing porosity, as observed in previous studies on the permeability of volcanic rocks [57,58], there is also substantial scatter within and between lithologies (Figure 6). For example, the permeability of samples with a porosity of ~40% can vary from ~2×10^{-16} to ~4×10^{-15} m^2 (Figure 6a). The relatively unaltered lava ballistics generally have lower porosity and permeability than the altered lava, altered ash tuff, and sulfur flow (Figure 6a). Compared to rocks collected from the surface (data from [13,59]; shown in grey on Figure 6a), the ballistic samples (yellow symbols on Figure 6a) generally have lower porosity and a narrower range of permeability. The samples with experimentally created tensile fractures are 4–5 orders of magnitude more permeable than the

unfractured rocks at both confining pressures of 1 and 3 MPa (Figure 6a,b). Irrespective of the initial permeability, the permeabilities of the fractured samples are very similar at low confining pressures (~10^{-12} m^2 at 1 and 3 MPa; Figure 6a,b).

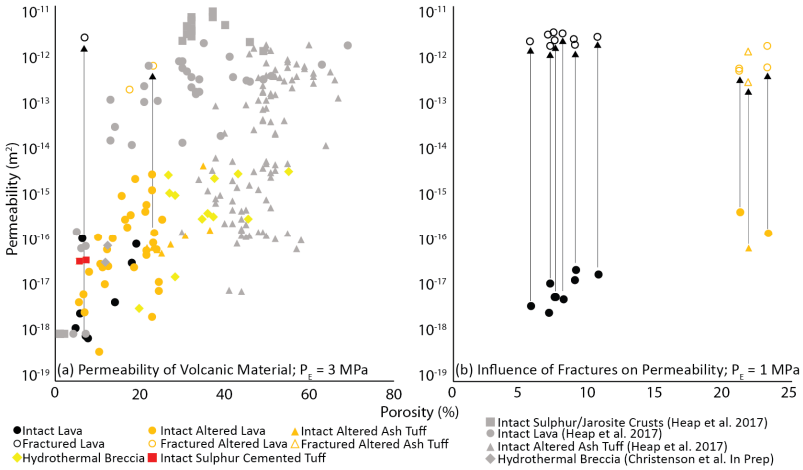

Figure 6. Permeability as a function of porosity at (**a**) confining pressure 3 MPa (this study) and 1 MPa, and (**b**) confining pressure 1 MPa showing the wide variability of matrix permeability (solid black points are unaltered intact lava from the edifice; yellow are altered intact ballistic samples collected at 3 MPa confining pressure) and low variability of fracture permeability (open points).

As confining pressure increases, the matrix permeability of the rocks decreases (Figure 7). A decrease in permeability as a function of increasing confining pressure has been previously reported in laboratory studies on volcanic rocks (e.g., [60,61]). The intact (i.e., without tensile fracture) altered samples have a higher permeability than the unaltered lava (Figure 7). An increase in confining pressure from 1 to 30 MPa leads to a decrease in permeability of ~1 order of magnitude in the unaltered lava and fractured unaltered lava, a decrease of 1-2 orders of magnitude in the unfractured altered lava, and a decrease in permeability of 2–4 orders of magnitude in the fractured altered lava (Figure 7). Importantly, our data show that the permeability reduction as confining pressure is greater in the fractured altered samples than in the fractured unaltered samples (Figure 7).

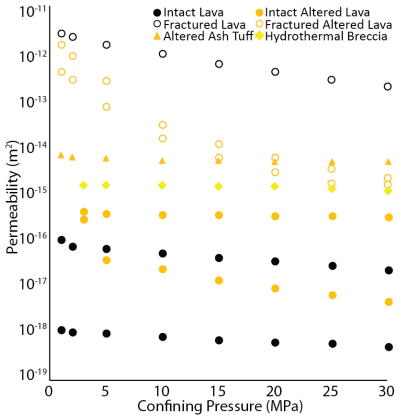

Figure 7. Permeability as a function of confining pressure showing the different impacts of confining pressure on altered and unaltered, fractured and unfractured samples.

Generally, our data show that uniaxial compressive strength (UCS) varies greatly over the range of porosity we tested. When combined with the other data from Whakaari [12] a clearer trend becomes evident in which UCS decreases as a function of increasing porosity (Figure 8), in agreement with previous studies on the strength of volcanic rocks (e.g., [62–64]). The observed decrease in UCS as a

function of porosity is not linear (Figure 8). The compressive strength data show a consistently low strength for samples containing >10% porosity (Figure 8). Low porosity unaltered lava is the strongest sublithology, while altered rocks are both more porous and weaker, and the sulfur cemented tuff is significantly weaker than the lava samples of similar porosity.

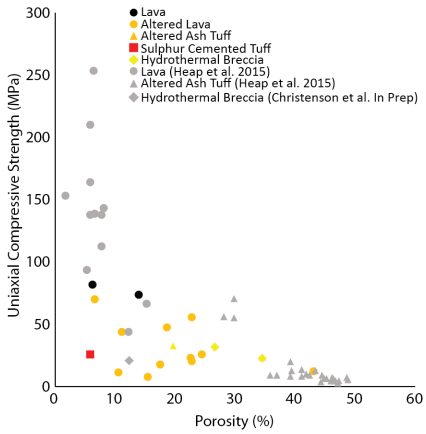

Figure 8. Uniaxial compressive strength (UCS) as a function of porosity for samples from this study and from [13,59].

3.3. Results Summary

The ballistics erupted from Whakaari are andesitic lavas, breccias, and tuffs. These rocks are all variably altered, containing silica polymorphs, alunite, and anhydrite. Many clasts show concentric alteration rinds. Anhydrite and alunite are common in pockets and veins, and they contain intercrystalline porosity, evidence for multiple cracking, veining, brecciation events, and cristobalite precipitation. In the tuff ballistics, it is difficult to distinguish matrix and clasts as both are recrystallized with silica polymorphs and alunite producing an overprinted microporosity. XRD results (Table 1) support the SEM interpretations, and additional analysis from the surge deposit shows dominantly cristobalite and plagioclase with little evidence of anhydrite and alunite. Consistent with previous data from surface rocks, tuff and altered lava ballistics are more porous and permeable than the less altered lavas. The permeability of the altered outer rind is generally higher when compared to the unaltered core of the same sample. When tensile fractures were created in cores, permeability increased by 4-6 orders of magnitude. However, the permeability of the fractured altered rocks decreases more than that of the fractured unaltered lava as confining pressure increases. Our results hint at the critical role fractures may play in the permeability of the altered rock that likely dominate the conduit at Whakaari.

4. Discussion

Our new laboratory data show that the permeability of our ballistic samples increases as a function of increasing porosity (Figure 6a), as observed in previous studies on the permeability of volcanic rocks (e.g., [57,58,65]) and porous sedimentary rocks (e.g., [66]). We also observe that a single tensile fracture in a laboratory sample can increase permeability by many orders of magnitude (Figure 6b). Similar to previous experiments [49] showed similar increases to permeability following the formation of a macroscopic fracture. Experiments performed at elevated pressures show that permeability decreases as a function of increasing confining pressure (Figure 7). We interpret this here as a result of the closure of pre-existing microcracks and high-aspect ratio pores within the samples, as concluded by previous studies that measured the permeability of microcracked volcanic rocks (e.g., [60,61]) and microcracked granite (e.g., [67]) as a function of increasing confining pressure. Finally, our uniaxial data show that the uniaxial compressive of our ballistic samples decreases as a function of increasing porosity (Figure 8), in agreement with previous studies on the strength of volcanic rocks (e.g., [62–64]).

Our new data allow us to assess the structure and composition of the breccia-filled conduit at Whakaari. The ballistic samples illustrate four distinct lithologies: (1) generally relatively unaltered lava blocks with thin alteration rinds, (2) completely or dominantly altered lava blocks, (3) completely altered tuffs, and (4) hydrothermal breccias. These lithologies represent the polylithic and variable breccia that comprise the conduit (Figure 9a).

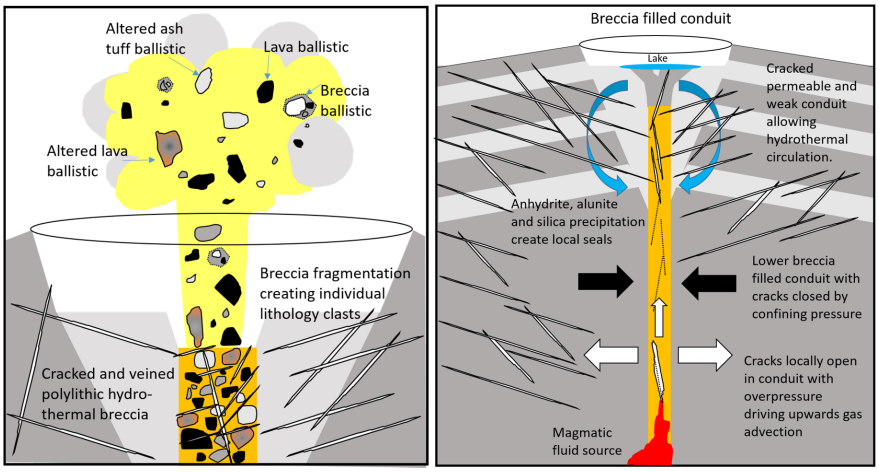

Figure 9. Proposed model of Whakaari conduit (**a**) near the surface and (**b**) eruption.

During an eruption, porous, weaker rocks are fragmented into smaller grain sizes [68] and therefore may be underrepresented in the block-sized ballistic samples. Soon after the 2016 eruption, the ash-sized component of the surge deposit had a generally yellow colour; however, our XRD analysis of the surge deposits indicates a dominantly altered cristobalite-rich composition. This indicates that the most fragmented component of the surge had a dominantly cristobalite mineralogy, and this likely comprised the finer grained dominantly tuff matrix of conduit-filling breccia which fragmented to form the surge and ballistics. Cristobalite was also observed in a dacitic bomb erupted at Whakaari in 1999 and is an inevitable product of shallow vapour phase alteration [69].

Several ballistic samples show evidence of brecciation and hydrothermal veining, with many samples also displaying anhydrite and alunite-bearing altered rims (Figures 3 and 5). The ballistic sample lithologies parallel those discussed in previous studies of the edifice of Whakaari: (1) altered tuffs composed of dominantly silica polymorphs and alunite and (2) relatively unaltered coherent lavas and breccias dominated by plagioclase and pyroxene (e.g., [12,14]. However, our data adds a third and fourth additional lithology, less common at the surface but dominant in the ballistics: (3) altered lavas dominated by anhydrite, and (4) hydrothermal breccias. We only found trace amounts of sulfur precipitation in the ballistics, indicating that sulfur-precipitated tuff may not be common in the subsurface.

We thus propose a model of a breccia-filled conduit containing clasts of dominantly altered lava and tuff in a matrix of relict ash-sized pyroclasts now replaced by silica polymorphs, alunite and anhydrite (Figure 9a). Similar to [13], we envisage that the conduit is surrounded by less altered coherent beds of lava, lava breccia, and tuff. Textural evidence in the ballistics and observations at the surface suggest that macrofractures are ubiquitous within the conduit and throughout the edifice, although these may be locally filled with alteration minerals such as anhydrite and alunite to form veins (Figure 9b). We acknowledge that some of the fractures present in the ballistics may be created during eruption, however, the overprinting of multiple fracture events recording in veining and mineralisation (Figure 5) show that fractures also develop pre-eruption in the conduit. Therefore, conduit itself may locally resemble a mineralised cockade breccia [35] but also contain facies similar to the heterolithic unbedded country rock breccia of maar diatremes [9] and the conduit beneath Unzen volcano [70]. Several vents were identified in the 2016 eruption [16] which support a model of a breccia filled vent system that diverges at shallow levels similar to that envisaged by [24].

5. Implications for Fluid Flow Monitoring and Eruption

At Whakaari, degassing occurs at distinct fumaroles, beneath the lake [21,22] and diffuse across the crater floor [71]. Macro- and microcracks are common in rocks collected at the surface [13]. Based on our data and previous studies [49], we estimate a fractured rock mass permeability of ~10^{-13} to ~10^{12} m^2 at the surface, away from open fumaroles. Our data also show that, for fractured samples, permeability in altered material is highly confining pressure-dependent, whereas the permeability in unaltered material is much less confining pressure-dependent. This relationship implies that permeability in the (highly fractured, altered) conduit is more confining pressure-dependent than the surrounding (less fractured, unaltered) edifice.

The effective pressure on any given part of the subsurface varies and is an interplay between depth (confining pressure) and pore pressure. Volcanoes in a state of unrest have variable pore pressures that frequently exceed confining pressures driving fluid flow, if pore pressure is greater than the tensile strength of the rock this can cause tensile failure (e.g., [12]) and if combined with a decompression event can drive fragmentation and eruption [14]. This is seen dramatically at Whakaari, which has been in an extended period of unrest and minor eruption since 2011. Outgassing and lake properties (temperature, chemistry, and level) vary significantly [21] and frequently shift on timeframes of hours to days, implying highly variable pore pressure, including periods where pore pressure exceeds confining pressure.

During recent unrest there were a range of surface phenomena, with several episodes of lake draining, mud fountaining and star bursting, ash venting [22] (Edwards et al., 2018), directed ballistic bursts and surges [16,18] (Chardot et al., 2014; Kilgour et al., 2019), and the appearance of a lava dome. Geophysics and satellite imagery show minor localised deformation and slope instability [32], significant tremor, and very long period (VLP) earthquakes [18,19]. Taken as a whole, these data reveal a model of shallow intrusions contributing time-variable heat and mass to the surface, along fumaroles and through eruptive vents. This model is consistent with the interpretation of gas advection as a mechanism to explain measured VLP activity [23]. Our interpretation of the eruptive vents as hydrothermally-cemented altered breccias with confining pressure-dependent permeability provides a mechanism to facilitate some of this time-dependent cycling behaviour.

Our observations indicate that cracks and veins are common in the ballistic rocks—something that we would expect from a conduit environment subjected to changing compressive and tensile stresses associated with intrusion and fluid movements. Our data suggest that pre-existing cracks in weaker hydrothermally mineralised zones easily close at confining pressures relevant for conduit processes. In unaltered rocks fractures may not fully close as asperities on crack surfaces may prop them open, maintaining permeability even at higher confining pressure. On long timescales of weeks to months these fractures allow eventual alteration and mineral replacement along these fluid flow pathways, and minerals may eventually crystallise within them to form veins. In contrast in the altered breccia-filled conduit, the weaker strength of hydrothermally mineralised fracture margins allow the asperities to be crushed, thus allowing closure under increased confining pressures, even on short timescales. This allows cracks to open and close as pressurized pore fluids open cracks and travel towards the surface (fluid advection; [23]). Once a fluid pulse has passed, pore pressures are reduced and the confining pressure recloses the fractures. In this manner, fractures can close instantaneously and reopen on timescales associated with gas advection. Hence, the opening and closing of the cracks is controlled by the accumulation of gas, sufficient to overcome confining pressure and generate a pore pressure. This allows time-variable advection of fluids, explaining the rapidly changing surface phenomena outlined in [22] and also the time variable tremor and very long period earthquakes described in ([18,23].

Effective pressure-controlled crack closure and permeability reduction are unlikely to build sufficient pore pressure to drive Whakaari's explosive events. Our data provide ample additional evidence for repeated fracture creation and mineral precipitation. Hydrothermally altered material in the conduit is generally weaker than the edifice forming rocks (Figure 8) and with tensile strengths of

3–5 MPa [59]. The generally weak and porous nature of the altered tuff and hydrothermally altered breccia implies it has a low fragmentation threshold [72] and would be susceptible to fragmentation due to phase-change related pressure fluctuations [14]. The dominance of the cristobalite in the surge matrix implies that it is composed of altered ash recycled from fine fragmentation of a porous tuff matrix [14]. There have been several different locations of vents on the lake floor [16] and the conduits are likely branching close to the surface with variable depths and types of mineralisation and resultant fragmentation histories similar to those envisaged at Okaro [24]. The frequency of explosive processes is on the order of weeks to years [18], which is sufficiently long to allow minerals to precipitate in veins and between breccia clasts in the conduits, resealing them. The exact conditions for this process are explained in [59]. Similar timescales for pressurisation as a result of alteration-induced reductions to permeability were proposed by [3]. Similar processes have been envisaged at other volcanoes [73]. However, here we offer an explanation for geophysical, geochemical, and visible changes that can occur in seconds to hours.

In conclusion, we provide evidence for a breccia-filled conduit of altered lava and tuff clasts dominantly cemented by alunite and anhydrite. The permeability of this altered material is susceptible to rapid variation in effective pressure allowing highly time-variable fluid advection, outgassing, and geophysical changes at the surface.

Supplementary Materials: An excel spreadsheet with all our data used for Figures 6–8 are available online at http://www.mdpi.com/2076-3263/10/4/138/s1.

Author Contributions: Conceptualization, B.M.K., M.C.V. and M.J.H.; methodology, B.M.K., M.C.V. and M.J.H.; formal analysis, A.F., R.H., S.M., M.C.V., T.R. and M.J.H.; investigation and experimentation, A.F., R.H., S.M., M.J.H., and T.R.; writing—original draft preparation, B.M.K., A.F., R.H., M.C.V., and M.J.H.; writing—review and editing, B.M.K., A.F., M.C.V., M.J.H., G.K., A.J., and B.C.; supervision, B.M.K., M.C.V. and M.J.H.; project administration, B.M.K.; funding acquisition, Sampling on the island was carried out by A.F., G.C., B.C. All authors have read and agreed to the published version of the manuscript.

Funding: This research was funded by New Zealand Ministry of Business, Innovation and Employment (MBIE) Strategic Science Investment Fund. M.J.H acknowledges an Erskine Teaching Fellowship awarded by the University of Canterbury.

Acknowledgments: We would like to acknowledge and thank White Island Tours, Frontiers Abroad, and the Green Room in aiding with the good times of data collection. Stephanie Gates and Ame McSporran also contributed useful discussion and data not directly used in the paper. Geoff Kilgour Bruce Christenson and Art Jolly were supported by the New Zealand Ministry of Business, Innovation and Employment (MBIE) Strategic Science Investment Fund. Shaun Mucalo assisted with SEM analysis.

Conflicts of Interest: The authors declare no conflict of interest. The funders had no role in the design of the study; in the collection, analyses, or interpretation of data; in the writing of the manuscript, or in the decision to publish the results.

References

1. Gardner, C.A.; White, R.A. Seismicity, gas emission and deformation from 18 July to 25 September 1995 during the initial phreatic phase of the eruption of Soufriere Hills Volcano, Montserrat. *Geol. Soc. Lond. Mem.* **2002**, *21*, 567–581. [CrossRef]
2. Norton, D.L.; Cathles, L.M. Breccia pipes, products of exsolved vapor from magmas. *Econ. Geol.* **1973**, *68*, 540–546. [CrossRef]
3. Heap, M.J.; Troll, V.R.; Kushnir, A.R.; Gilg, H.A.; Collinson, A.S.; Deegan, F.M.; Darmawan, H.; Seraphine, N.; Neuberg, J.; Walter, T.R. Hydrothermal alteration of andesitic lava domes can lead to explosive volcanic behaviour. *Nat. Commun.* **2019**, *10*, 1–10. [CrossRef] [PubMed]
4. Schauroth, J.; Wadsworth, F.B.; Kennedy, B.; von Aulock, F.W.; Lavallée, Y.; Damby, D.E.; Dingwell, D.B. Conduit margin heating and deformation during the AD 1886 basaltic Plinian eruption at Tarawera volcano, New Zealand. *Bull. Volcanol.* **2016**, *78*, 12. [CrossRef] [PubMed]
5. Stasiuk, M.V.; Barclay, J.; Carroll, M.R.; Jaupart, C.; Ratté, J.C.; Sparks, R.S.J.; Tait, S.R. Degassing during magma ascent in the Mule Creek vent (USA). *Bull. Volcanol.* **1996**, *58*, 117–130. [CrossRef]
6. Tuffen, H.; Dingwell, D. Fault textures in volcanic conduits: Evidence for seismic trigger mechanisms during silicic eruptions. *Bull. Volcanol.* **2005**, *67*, 370–387. [CrossRef]

7. Wadsworth, F.B.; Kennedy, B.M.; Branney, M.J.; von Aulock, F.W.; Lavallée, Y.; Menendez, A. Exhumed conduit records magma ascent and drain-back during a Strombolian eruption at Tongariro volcano, New Zealand. *Bull. Volcanol.* **2015**, *77*, 71. [CrossRef]
8. White, J.D.; Ross, P.S. Maar-diatreme volcanoes: A review. *J. Volcanol. Geotherm. Res.* **2011**, *201*, 1–29. [CrossRef]
9. Lefebvre, N.S.; White, J.D.L.; Kjarsgaard, B.A. Unbedded diatreme deposits reveal maar-diatreme-forming eruptive processes: Standing Rocks West, Hopi Buttes, Navajo Nation, USA. *Bull. Volcanol.* **2013**, *75*, 739. [CrossRef]
10. Zhang, J.Q.; Li, S.R.; Santosh, M.; Luo, J.Y.; Li, C.L.; Song, J.Y.; Lu, J.; Liang, X. The genesis and gold mineralization of the crypto-explosive breccia pipe in the Yixingzhai gold region, central North China Craton. *Geol. J.* **2019**. [CrossRef]
11. Omosanya, K.O.; Eruteya, O.E.; Siregar, E.S.; Zieba, K.J.; Johansen, S.E.; Alves, T.M.; Waldmann, N.D. Three-dimensional (3-D) seismic imaging of conduits and radial faults associated with hydrothermal vent complexes (Vøring Basin, Offshore Norway). *Mar. Geol.* **2018**, *399*, 115–134. [CrossRef]
12. Heap, M.J.; Kennedy, B.M.; Pernin, N.; Jacquemard, L.; Baud, P.; Farquharson, J.I.; Scheu, B.; Lavallée, Y.; Gilg, H.A.; Letham-Brake, M.; et al. Mechanical behaviour and failure modes in the Whakaari (White Island volcano) hydrothermal system, New Zealand. *J. Volcanol. Geotherm. Res.* **2015**, *295*, 26–42. [CrossRef]
13. Heap, M.J.; Kennedy, B.M.; Farquharson, J.I.; Ashworth, J.; Mayer, K.; Letham-Brake, M.; Reuschlé, T.; Gilg, H.A.; Scheu, B.; Lavallée, Y.; et al. A multidisciplinary approach to quantify the permeability of the Whakaari/White Island volcanic hydrothermal system (Taupo Volcanic Zone, New Zealand). *J. Volcanol. Geotherm. Res.* **2017**, *332*, 88–108. [CrossRef]
14. Mayer, K.; Scheu, B.; Gilg, H.A.; Heap, M.J.; Kennedy, B.M.; Lavallée, Y.; Letham-Brake, M.; Dingwell, D.B. Experimental constraints on phreatic eruption processes at Whakaari (White Island volcano). *J. Volcanol. Geotherm. Res.* **2015**, *302*, 150–162. [CrossRef]
15. Kennedy, B.; Spieler, O.; Scheu, B.; Kueppers, U.; Taddeucci, J.; Dingwell, D.B. Conduit implosion during Vulcanian eruptions. *Geology* **2005**, *33*, 581–584. [CrossRef]
16. Kilgour, G.N.; Gates, S.; Kennedy, B.; Farquhar, A.; McSporran, A.; Asher, C. Phreatic eruption dynamics derived from deposit analysis: A case study from a small, phreatic eruption from Whakāri/White Island, New Zealand. *Earth Planets Space* **2019**, *71*, 36. [CrossRef]
17. Houghton, B.F.; Nairn, I.A. The 1976–1982 Strombolian and phreatomagmatic eruptions of White Island, New Zealand: Eruptive and depositional mechanisms at a 'wet' volcano. *Bull. Volcanol.* **1991**, *54*, 25–49. [CrossRef]
18. Chardot, L.; Jolly, A.D.; Kennedy, B.M.; Fournier, N.; Sherburn, S. Using volcanic tremor for eruption forecasting at White Island volcano (Whakaari), New Zealand. *J. Volcanol. Geotherm. Res.* **2015**, *302*, 11–23. [CrossRef]
19. Jolly, A.; Lokmer, I.; Christenson, B.; Thun, J. Relating gas ascent to eruption triggering for the April 27, 2016, White Island (Whakaari), New Zealand eruption sequence. *Earth Planets Space* **2018**, *70*, 1–15. [CrossRef]
20. Fournier, N.; Chardot, L. Understanding volcano hydrothermal unrest from geodetic observations: Insights from numerical modeling and application to White Island volcano, New Zealand. *J. Geophys. Res. Solid Earth* **2012**, *117*. [CrossRef]
21. Christenson, B.W.; White, S.; Britten, K.; Scott, B.J. Hydrological evolution and chemical structure of a hyper-acidic spring-lake system on Whakaari/White Island, NZ. *J. Volcanol. Geotherm. Res.* **2017**, *346*, 180–211. [CrossRef]
22. Edwards, M.J.; Kennedy, B.M.; Jolly, A.D.; Scheu, B.; Jousset, P. Evolution of a small hydrothermal eruption episode through a mud pool of varying depth and rheology, White Island, NZ. *Bull. Volcanol.* **2017**, *79*, 16. [CrossRef]
23. Jolly, A.D.; Chardot, L.; Neuberg, J.; Fournier, N.; Scott, B.J.; Sherburn, S. High impact mass drops from helicopter: A new active seismic source method applied in an active volcanic setting. *Geophys. Res. Lett.* **2012**, *39*. [CrossRef]
24. Montanaro, C.; Cronin, S.; Scheu, B.; Kennedy, B.; Scott, B. Complex crater fields formed by steam-driven eruptions: Lake Okaro, New Zealand. *GSA Bull.* **2020**. [CrossRef]
25. Chouet, B.A. Long-period volcano seismicity: Its source and use in eruption forecasting. *Nature* **1996**, *380*, 309–316. [CrossRef]

26. McNutt, S.R. Seismic monitoring and eruption forecasting of volcanoes: A review of the state-of-the-art and case histories. In *Monitoring and Mitigation of Volcano Hazards*; Springer: Berlin/Heidelberg, Germany, 1996; pp. 99–146.
27. Sparks, R.S.J. Forecasting volcanic eruptions. *Earth Planet. Sci. Lett.* **2003**, *210*, 1–15. [CrossRef]
28. Brenguier, F.; Shapiro, N.M.; Campillo, M.; Ferrazzini, V.; Duputel, Z.; Coutant, O.; Nercessian, A. Towards forecasting volcanic eruptions using seismic noise. *Nat. Geosci.* **2008**, *1*, 126–130. [CrossRef]
29. Bell, A.F.; Greenhough, J.; Heap, M.J.; Main, I.G. Challenges for forecasting based on accelerating rates of earthquakes at volcanoes and laboratory analogues. *Geophys. J. Int.* **2011**, *185*, 718–723. [CrossRef]
30. Bean, C.J.; De Barros, L.; Lokmer, I.; Métaxian, J.P.; O'Brien, G.; Murphy, S. Long-period seismicity in the shallow volcanic edifice formed from slow-rupture earthquakes. *Nat. Geosci.* **2014**, *7*, 71–75. [CrossRef]
31. Clarke, J.; Adam, L.; Sarout, J.; van Wijk, K.; Kennedy, B.; Dautriat, J. The relation between viscosity and acoustic emissions as a laboratory analogue for volcano seismicity. *Geology* **2019**, *47*, 499–503. [CrossRef]
32. Hamling, I.J. Crater Lake controls on volcano stability: Insights from White Island, New Zealand. *Geophys. Res. Lett.* **2017**, *44*, 11–311. [CrossRef]
33. Todesco, M.; Rinaldi, A.P.; Bonafede, M. Modeling of unrest signals in heterogeneous hydrothermal systems. *J. Geophys. Res. Solid Earth* **2010**, *115*. [CrossRef]
34. Pola, A.; Crosta, G.; Fusi, N.; Barberini, V.; Norini, G. Influence of alteration on physical properties of volcanic rocks. *Tectonophysics* **2012**, *566*, 67–86. [CrossRef]
35. Sruoga, P.; Rubinstein, N. Processes controlling porosity and permeability in volcanic reservoirs from the Austral and Neuquén basins, Argentina. *AAPG Bull.* **2007**, *91*, 115–129. [CrossRef]
36. Wyering, L.D.; Villeneuve, M.C.; Wallis, I.C.; Siratovich, P.A.; Kennedy, B.M.; Gravley, D.M.; Cant, J.L. Mechanical and physical properties of hydrothermally altered rocks, Taupo Volcanic Zone, New Zealand. *J. Volcanol. Geotherm. Res.* **2014**, *288*, 76–93. [CrossRef]
37. Mordensky, S.P.; Villeneuve, M.C.; Kennedy, B.M.; Heap, M.J.; Gravley, D.M.; Farquharson, J.I.; Reuschlé, T. Physical and mechanical property relationships of a shallow intrusion and volcanic host rock, Pinnacle Ridge, Mt. Ruapehu, New Zealand. *J. Volcanol. Geotherm. Res.* **2018**, *359*, 18–20. [CrossRef]
38. Mordensky, S.P.; Heap, M.J.; Kennedy, B.M.; Gilg, H.A.; Villeneuve, M.C.; Farquharson, J.I.; Gravley, D.M. Influence of alteration on the mechanical behaviour and failure mode of andesite: Implications for shallow seismicity and volcano monitoring. *Bull. Volcanol.* **2019**, *81*, 44. [CrossRef]
39. Heap, M.J.; Gravley, D.M.; Kennedy, B.M.; Gilg, H.A.; Bertolett, E.; Barker, S.L. Quantifying the role of hydrothermal alteration in creating geothermal and epithermal mineral resources: The Ohakuri ignimbrite (Taupō Volcanic Zone, New Zealand). *J. Volcanol. Geotherm. Res.* **2020**, *390*, 106703. [CrossRef]
40. Cant, J.L.; Siratovich, P.A.; Cole, J.W.; Villeneuve, M.C.; Kennedy, B.M. Matrix permeability of reservoir rocks, Ngatamariki geothermal field, Taupo Volcanic Zone, New Zealand. *Geotherm. Energy* **2018**, *6*, 2. [CrossRef]
41. Farquharson, J.I.; Wild, B.; Kushnir, A.R.; Heap, M.J.; Baud, P.; Kennedy, B. Acid-induced dissolution of andesite: Evolution of permeability and strength. *J. Geophys. Res. Solid Earth* **2019**, *124*, 257–273. [CrossRef]
42. Heap, M.J.; Farquharson, J.I.; Baud, P.; Lavallée, Y.; Reuschlé, T. Fracture and compaction of andesite in a volcanic edifice. *Bull. Volcanol.* **2015**, *77*, 55. [CrossRef] [PubMed]
43. Siratovich, P.A.; Heap, M.J.; Villeneuve, M.C.; Cole, J.W.; Kennedy, B.M.; Davidson, J.; Reuschlé, T. Mechanical behaviour of the Rotokawa Andesites (New Zealand): Insight into permeability evolution and stress-induced behaviour in an actively utilised geothermal reservoir. *Geothermics* **2016**, *64*, 163–179. [CrossRef]
44. Ogata, K.; Senger, K.; Braathen, A.; Tveranger, J. Fracture corridors as seal-bypass systems in siliciclastic reservoir-cap rock successions: Field-based insights from the Jurassic Entrada Formation (SE Utah, USA). *J. Struct. Geol.* **2014**, *66*, 162–187. [CrossRef]
45. von Aulock, F.W.; Nichols, A.R.L.; Kennedy, B.M.; Oze, C. Timescales of texture development in a cooling lava dome. *Geochim. Cosmochim. Acta* **2013**, *114*, 72–80. [CrossRef]
46. Saubin, E.; Kennedy, B.; Tuffen, H.; Villeneuve, M.; Davidson, J.; Burchardt, S. Comparative field study of shallow rhyolite intrusions in Iceland: Emplacement mechanisms and impact on country rocks. *J. Volcanol. Geotherm. Res.* **2019**, *388*, 106691. [CrossRef]
47. Siratovich, P.; Villeneuve, M.; Cole, J.; Kennedy, B.; Bégué, F. Saturated heating and quenching of three crustal rocks and implications for thermal stimulation of permeability in geothermal reservoirs. *Int. J. Rock. Mech. Min.* **2015**, *80*, 265–280. [CrossRef]

48. Mordensky, S.; Kennedy, B.; Villeneuve, M.; Lavallée, Y.; Reichow, M.; Wallace, P.; Siratovich, P.; Gravley, D. Increasing the Permeability of Hydrothermally Altered Andesite by Transitory Heating. *Geochem. Geophys. Geosyst.* **2019**, *20*, 5251–5269. [CrossRef]
49. Heap, M.J.; Kennedy, B.M. Exploring the scale-dependent permeability of fractured andesite. *Earth Planet. Sci. Lett.* **2016**, *447*, 139–150. [CrossRef]
50. Lamur, A.; Kendrick, J.E.; Eggertsson, G.H.; Wall, R.J.; Ashworth, J.D.; Lavallée, Y. The permeability of fractured rocks in pressurised volcanic and geothermal systems. *Sci. Rep.* **2017**, *7*, 6173. [CrossRef]
51. Eggertsson, G.H.; Lavallée, Y.; Kendrick, J.E.; Markússon, S.H. Improving fluid flow in geothermal reservoirs by thermal and mechanical stimulation: The case of Krafla volcano, Iceland. *J. Volcanol. Geotherm. Res.* **2018**, *391*. [CrossRef]
52. Mordensky, S.P.; Villeneuve, M.C.; Farquharson, J.I.; Kennedy, B.M.; Heap, M.J.; Gravley, D.M. Rock mass properties and edifice strength data from Pinnacle Ridge, Mt. Ruapehu, New Zealand. *J. Volcanol. Geotherm. Res.* **2018**, *367*, 46–62. [CrossRef]
53. Farquhar, A. Ballistic Analysis Inferring Subsurface Hydrothermal Alteration and Mineralogical Seal Control on Eruptions at Whakaari Volcano, New Zealand. Colorado College: Colorado Springs, CO, USA, 2018; unpublished.
54. Deligne, N.I.; Jolly, G.E.; Taig, T.; Webb, T.H. Evaluating life-safety risk for fieldwork on active volcanoes: The volcano life risk estimator (VoLREst), a volcano observatory's decision-support tool. *J. Appl. Volcanol.* **2018**, *7*, 7. [CrossRef]
55. Heap, M.J.; Kushnir, A.R.; Gilg, H.A.; Wadsworth, F.B.; Reuschlé, T.; Baud, P. Microstructural and petrophysical properties of the Permo-Triassic sandstones (Buntsandstein) from the Soultz-sous-Forêts geothermal site (France). *Geotherm. Energy* **2017**, *5*, 26. [CrossRef]
56. Cole, J.W.; Thordarson, T.; Burt, R.M. Magma origin and evolution of White Island (Whakaari) volcano, Bay of plenty, New Zealand. *J. Pet.* **2000**, *41*, 867–895. [CrossRef]
57. Farquharson, J.; Heap, M.J.; Varley, N.R.; Baud, P.; Reuschlé, T. Permeability and porosity relationships of edifice-forming andesites: A combined field and laboratory study. *J. Volcanol. Geotherm. Res.* **2015**, *297*, 52–68. [CrossRef]
58. Wadsworth, F.B.; Vasseur, J.; Scheu, B.; Kendrick, J.E.; Lavallée, Y.; Dingwell, D.B. Universal scaling of fluid permeability during volcanic welding and sediment diagenesis. *Geology* **2016**, *44*, 219–222. [CrossRef]
59. Christenson, B.W.; Kennnedy, B.M.; Reyes, A.G.; Farquahar, A.; Heap, M.J.; Henley, R.W. Permeability reduction and other processes leading to phreatic eruptions from wet volcanic systems: Insights from the 27 April 2016 eruption from White Island, New Zealand. *Geophys. Res. Abstr.* **2019**, *21*, 1.
60. Vinciguerra, S.; Trovato, C.; Meredith, P.G.; Benson, P.M. Relating seismic velocities, thermal cracking and permeability in Mt. Etna and Iceland basalts. *Int. J. Rock Mech. Min. Sci.* **2005**, *42*, 900–910. [CrossRef]
61. Nara, Y.; Meredith, P.G.; Yoneda, T.; Kaneko, K. Influence of macro-fractures and micro-fractures on permeability and elastic wave velocities in basalt at elevated pressure. *Tectonophysics* **2011**, *503*, 52–59. [CrossRef]
62. Al-Harthi, A.A.; Al-Amri, R.M.; Shehata, W.M. The porosity and engineering properties of vesicular basalt in Saudi Arabia. *Eng. Geol.* **1999**, *54*, 313–320. [CrossRef]
63. Heap, M.J.; Xu, T.; Chen, C.F. The influence of porosity and vesicle size on the brittle strength of volcanic rocks and magma. *Bull. Volcanol.* **2014**, *76*, 856. [CrossRef]
64. Schaefer, L.N.; Kendrick, J.E.; Oommen, T.; Lavallée, Y.; Chigna, G. Geomechanical rock properties of a basaltic volcano. *Front. Earth Sci.* **2015**, *3*, 29. [CrossRef]
65. Kushnir, A.R.; Martel, C.; Bourdier, J.L.; Heap, M.J.; Reuschlé, T.; Erdmann, S.; Komorowski, J.C.; Cholik, N. Probing permeability and microstructure: Unravelling the role of a low-permeability dome on the explosivity of Merapi (Indonesia). *J. Volcanol. Geotherm. Res.* **2016**, *316*, 56–71. [CrossRef]
66. Bourbie, T.; Zinszner, B. Hydraulic and acoustic properties as a function of porosity in Fontainebleau sandstone. *J. Geophys. Res. Solid Earth* **1985**, *90*, 11524–11532. [CrossRef]
67. Darot, M.; Guéguen, Y.; Baratin, M.L. Permeability of thermally cracked granite. *Geophys. Res. Lett.* **1992**, *19*, 869–872. [CrossRef]
68. Kueppers, U.; Scheu, B.; Spieler, O.; Dingwell, D.B. Fragmentation efficiency of explosive volcanic eruptions: A study of experimentally generated pyroclasts. *J. Volcanol. Geotherm. Res.* **2006**, *153*, 125–135. [CrossRef]

69. Schipper, C.I.; Mandon, C.; Maksimenko, A.; Castro, J.M.; Conway, C.E.; Hauer, P.; Kirilova, M.; Kilgour, G. Vapor-phase cristobalite as a durable indicator of magmatic pore structure and halogen degassing: An example from White Island volcano (New Zealand). *Bull. Volcanol.* **2017**, *79*, 74. [CrossRef]
70. Goto, Y.; Nakada, S.; Kurokawa, M.; Shimano, T.; Sugimoto, T.; Sakuma, S.; Hoshizumi, H.; Yoshimoto, M.; Uto, K. Character and origin of lithofacies in the conduit of Unzen volcano, Japan. *J. Volcanol. Geotherm. Res.* **2008**, *175*, 45–59. [CrossRef]
71. Bloomberg, S.; Rissmann, C.; Mazot, A.; Oze, C.; Horton, T.; Gravley, D.; Kennedy, B.; Werner, C.; Christenson, B.; Pawson, J. Soil Gas Flux Exploration at the Rotokawa Geothermal Field and White Island, New Zealand. In Proceedings of the Thirty Sixth Workshop on Geothermal Reservoir Engineering, Stanford, CA, USA, 30 January–1 February 2012; Volume 30.
72. Spieler, O.; Kennedy, B.; Kueppers, U.; Dingwell, D.B.; Scheu, B.; Taddeucci, J. The fragmentation threshold of pyroclastic rocks. *Earth Planet. Sci. Lett.* **2004**, *226*, 139–148. [CrossRef]
73. Caudron, C.; Taisne, B.; Neuberg, J.; Jolly, A.D.; Christenson, B.; Lecocq, T.; Syahbana, D.; Suantika, G. Anatomy of phreatic eruptions. *Earth Planets Space* **2018**, *70*, 168. [CrossRef]